Temperature-Insensitive Resonant Strain Sensor

Xintian Liu, Qianyi Xie, Alper Ozgurluk, and Clark T.-C. Nguyen

Berkeley Sensor & Actuator Center (BSAC), Dept. of EECS
University of California at Berkeley, Berkeley, California, USA
xintian.liu@berkeley.edu

***Abstract*—Electrical stiffnesses generated within capacitive transducer gaps that differentially straddle the edges of a single micromechanical spoke-supported ring resonator enable a tiny strain sensor that occupies only 0.002mm², so far measures strain changes as small as 491nε, and posts an output strain temperature coefficient of only 0.1με/°C at 40°C, which is 40 times better than achievable by a polysilicon piezoresistive strain gauge and 3 times better than the nearest competing resonant strain sensor. The key to this temperature insensitivity rests in the use of a fully differential ring resonator and a curve-fitting method to extract gap differences that suppresses the false output due to Young's modulus temperature changes, making it quite compelling for structural health monitoring of surfaces operating in harsh environments, such as in automotive applications.**

***Keywords*—MEMS, strain gauge, resonator, VHF, quality factor, ring, temperature.**

I. Introduction

Structural health monitoring for portable applications, such as hydrogen tanks on future fuel cell-powered vehicles, call for surface areal coverage by miniature sensors capable of operating in harsh environments. This fuels a need for simultaneous small size, high resolution, and temperature insensitivity. Here, conventional resistive foil strain gauges fall short with typical resolution on the order of 10με [1] and gauge factor temperature sensitivity of 50 με/°C [2]. With compensation, the temperature insensitivity can improve to -17 με/°C [2], but this sensor type still consumes a rather large areal footprint on the order of 100 mm² [3]. Resonant strain gauges fare much better and if realized via MEMS technology [4] [5] [6] can achieve tiny size, resolutions approaching 100 nε [4], and improved temperature stability, where Young's modulus temperature dependence yields scale factor temperature coefficients in the range of 0.3 με/°C [5]. Addition of an orthogonally oriented identical resonator offers a method for improving temperature insensitivity, but at the cost of complexity, area, and the inability to measure strain in two directions simultaneously [6].

This work employs electrical stiffness generated by capacitive transducer gaps that differentially straddle the edges of a single micromechanical spoke-supported ring resonator [7] pictured in Fig. 1 to achieve a strain sensor that bests even resonant counterparts in size, resolution, and temperature stability. Its use of a fully differential ring and a curve-fitting method to extract gap difference suppresses false outputs due to environmental temperature changes, making it more compelling for harsh environments.

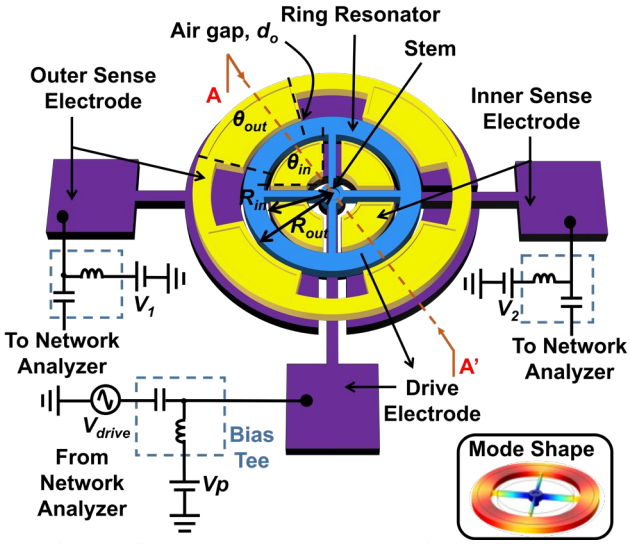

Fig. 1: The polysilicon ring resonator strain sensor described herein in a typical test circuit with critical dimensions labeled and mode shape.

II. Polysilicon Ring Resonator Strain Gauge

As shown in Fig. 1, the strain sensor herein comprises a phosphorous-doped polysilicon ring resonator supported by four spokes that converge to a center anchor. Inner and outer doped polysilicon electrodes surround the ring, spaced 80 nm from its sidewalls. This specific design electrically connects all inner electrodes, which share the same access bond pad. Likewise for all outer electrodes. Note that the electrodes can alternatively be electrically separated to allow for more general dimensional strain sensing, e.g., sensing along two axes. As configured in Fig. 1, however, the sensor senses isotropic strain.

A. Resonance-Inspired Sensing Mechanism

Fig. 1 indicates the electrical connection required to operate this device as an electrical-stiffness-based strain sensor. This configuration mimics that needed to measure the frequency response of the device with additional provisions to allow measurement of frequency differences along different transducer paths, i.e., along the inner electrode-to-resonator path versus the outer one. Here, the AC force needed to excite the ring into resonance vibration in its fundamental radial mode (depicted in the inset of Fig. 1) requires a combination of an AC input signal and a DC bias that effectively amplifies the AC force at its fundamental frequency. When driving from the ring bond pad as shown in Fig. 1, taking the output from the inner electrode bond pad yields the frequency response of the inner electrode-to-resonator path. Likewise, the outer path response results when

sensing via the outer electrode bond pad. Both electrodes and the ring connect to separate DC power supplies via three bias-tees.

The different DC voltages across different transducing gaps, i.e., inner and outer, modify the resonance frequency of the resonator via electrical stiffness [8] according to

$$f_{in(out)} = \frac{1}{2\pi}\sqrt{\frac{k_m - k_e}{m_m}} = \sqrt{f_{nom}^2 - \frac{\varepsilon_0 (V_p - V_i)^2}{2\pi^3 \rho W R}\frac{R_{in(out)}\theta_{in(out)}}{\chi_{in(out)} d_{in(out)}^3}} \quad (1)$$

Where k_m and k_e are mechanical stiffness and electrical stiffness respectively, m_m is the equivalent mass of the ring, i is 1 or 2, V_1, V_2, V_P are the DC voltages applied to the inner electrode, the outer electrode, and the polysilicon ring, respectively, W is the annulus width, $R_{in(out)}$ is the distance from inner(outer) edges of ring to the center stem, R is the average of R_{in} and R_{out}, $d_{in(out)}$ is the inner(outer) electrode actuation gap, $\theta_{in(out)}$ is the inner(outer) electrode span angle in radians, $\chi_{in(out)}$ is the factor modifying the physical mass of the ring when it vibrates in its first mode (*cf.* Fig. 1) [9], and f_{nom} is the nominal resonance frequency of the ring (with no voltages applied), given by

$$f_{nom} = \frac{p}{2\pi}\sqrt{\frac{E}{\rho(1-\sigma^2)}} \quad (2)$$

where p is a frequency determined by the dimensions of the resonator [9], and E, ρ and σ are the Young's modulus, density, and planar Poisson ratio of the structural material, respectively.

Unfortunately, among the variables in ((**1**), the Young's modulus can be quite temperature sensitive [10] and often dominates the temperature dependence of the overall resonance frequency. For example, the Young's modulus of silicon has a temperature coefficient of -52.6 ppm/°C near room temperature. This means a resonant strain gauge utilizing the resonance frequency shift of a double-anchored silicon beam resonator to detect strain would suffer a false output on any temperature shift, on the order of 1.8 με/°C if the sensor has a strain gauge sensitivity of 15 ppm/με. Thus, while resonant strain sensors do outperform conventional resistive foil sensors by a significant margin in temperature insensitivity, there is room for improvement if the dependence on Young's modulus can be removed.

B. Strain Gauge Working Principle

To suppress temperature sensitivity, the ring resonator strain gauge of Fig. 1 does not utilize resonance frequency as a direct readout for strain. Rather, it employs resonance properties to measure applied strain via accurate determination of strain-induced shifts to its inner and outer electrode-to-resonator transducer gaps and using the difference between inner and outer gap changes to null out common-mode errors.

To expand on this, Fig. 2 (a) presents the cross-section view of the ring resonator along A-A′ in Fig. 1 without applied strain. Ideally, the difference between the inner and the outer gap is $\Delta d = d_{in}$-d_{out} immediately after release and before application of external stress would be zero. However, residual stress between the polysilicon and substrate before release [7] generally imposes a starting no-strain gap difference. When the substrate experiences an external tensile strain (perhaps induced by the surface to which it is attached/glued), the cross-section of Fig. 2(b) ensues, where the ring resonator does not deform, thanks to its center-only anchoring to the substrate, while both inner and outer electrodes move away from the center of the ring. As a result, one gap expands and the other shrinks. If a method is available that can accurately determine the gap distances, the substrate strain due to external stress follows from

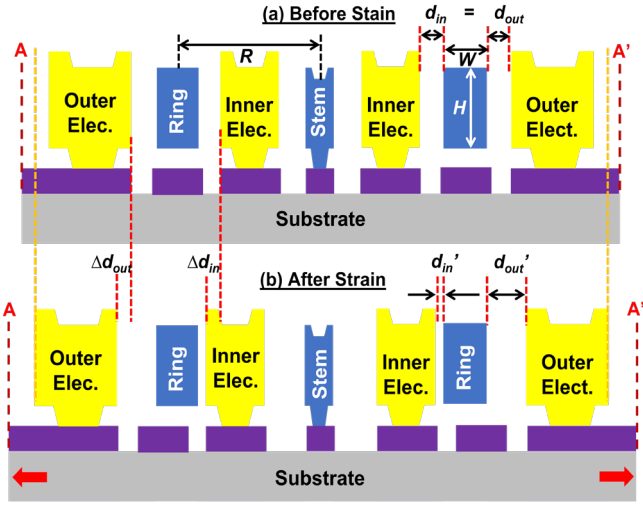

Fig. 2: Cross-section through AA' in Fig. 1 (a) before and (b) after the substrate experiences tensile strain.

$$\varepsilon = \frac{\Delta d' - \Delta d}{2R} \quad (3)$$

where Δd is the gap difference d_{in}-d_{out} after fabrication, immediately after release and before the application of external strain, and $\Delta d'$ is the gap difference after the applied strain.

Equation (3) indicates that the resolution of strain sensing depends primarily on the accuracy by which the gaps can be determined. This is where electrical stiffness becomes instrumental to not only enabling superior strain measurement, but also to ensuring resilience against temperature-derived false outputs.

C. Electrical Stiffness-Based Gap Extraction

Equation (1) indicates a strong third power dependence of the ring resonance frequency on electrode-to-resonator gap spacing. This suggests that a very accurate determination of gap spacing might be obtained by curve-fitting measured curves of frequency versus DC bias (V_P-V_i) using (1), where a match ensues when the right value of gap spacing $d_{in(out)}$ is used.

While the stated third power dependence of resonance frequency shift on electrode-to-resonator gap provides a very accurate means by which to determine the gap spacing, the question remains whether this method provides temperature independence? That it does indeed is readily apparent upon rearrangement of (1) to yield

$$f_{in(out)}^2 = f_{nom}^2 - k\frac{\left(V_p - V_i\right)^2}{d_{in(out)}^3} \quad (4)$$

where

$$k = \frac{\varepsilon_0}{2\pi^3 \rho W R}\frac{R_{in(out)}\theta_{in(out)}}{\chi_{in(out)}} \quad (5)$$

is a parameter that does not depend on Young's modulus, but rather on other material properties and resonator geometries that have much smaller temperature dependence. Here, the first term on the right side, i.e., the nominal resonance frequency f_{nom}^2, captures completely the influence of the Young's modulus, while the second is independent of it.

The observation that the first term is merely the y-axis intercept on a plot of $f_{in(out)}^2$ versus $(V_P\text{-}V_i)^2$, while the plot slope depends strongly on gap spacing $d_{in(out)}$, reveals the utility of such a plot towards accurate and relatively temperature-independent determination of gap spacing. Specifically, the transducing electrode-to-resonator gap $d_{in(out)}$ may be extracted by plotting the measured $f_{in(out)}^2$ versus the applied $(V_P\text{-}V_i)^2$, then finding the slope of the line. Dividing the slope of the fitted curve by k yields the value of the transducing gap. The nominal frequency appears in the $f_{in(out)}^2$ versus $(V_P\text{-}V_i)^2$ plot as an offset term and does not affect the gap-determining slope of the curve, so does not corrupt gap extraction.

Alternatively, the gap spacing $d_{in(out)}$ can be determined by curve-fitting a plot of $f_{in(out)}$ versus $(V_P\text{-}V_i)$, where the need to match the nuances of curvature might yield a more accurate value.

It should be noted that (5) is not completely independent of temperature. Rather, the ring resonator dimensions change with temperature and can influence the gap spacing if there are finite differences between the thermal expansion coefficient of polysilicon and that of the underlying silicon substrate. For example, the expression for the change in inner gap spacing Δd_{in} due to a temperature shift ΔT is

$$\Delta d_{in} = (\alpha_r - \alpha_s) R_{in} \Delta T \quad (6)$$

where α_r and α_s are thermal expansion coefficient of structural and substrate materials, respectively. To suppress this residual temperature sensitivity, it is best to match the thermal expansion coefficients for structure and substrate as closely as possible. While the polysilicon structural material used here is a good match to the single-crystal silicon substrate, it is not a perfect match. The use of silicon structural material would likely fare better.

In addition to matching structure and substrate materials to null false outputs due to local thermal expansion, many applications prefer to also null thermal expansion strain in the surface experiencing the strain to be measured, i.e., to measure only non-thermal strain. Here, the available set of micro machinable materials provides ample opportunity to match the thermal behavior of the sensor resonator element to the measured surface, allowing the sensor and surface to expand identically with temperature to null out the surface's thermal expansion strain.

Ultimately, the accuracy of electrode-to-resonator gap extraction depends on the accuracy of frequency measurement to generate the frequency versus DC bias curves that govern curve-fitting. This in turn depends on the short-term frequency stability of ring's resonance frequency, which improves with the use of positive feedback to self-sustain oscillation during frequency measurement. (Note, however, that the experimental results obtained herein use open-loop data, so perhaps are less accurate than otherwise possible.)

TABLE I RING GEOMETRIC DIMENSIONS AND MATERIAL PROPERTIES

Parameter	Value	Parameter	Value
Inner Radius, R_{in}	11.5μm	Outer Radius, R_{out}	17.4μm
Inner Gap, d_{in}	80nm	Outer Gap, d_{out}	80nm
Inner/Outer Elect. Angle, θ_{in}	65.25°	Young's modulus, E	158GPa
Inner Coeff., χ_{in}	0.912	Outer Coeff., χ_{out}	1.075
Freq. Param., p	68297.2	Thickness, H	3μm
Density, ρ	2300kg/m^3	Poisson Ratio, σ	0.226

The ultimate dynamic range of strain measurement comes down to the dimensions of the gap and ring radius, where dimensions must be chosen so that the largest expected strain does not induce touching (i.e., shorting) of any electrode to the resonator structure. For example, it would take 200-nm inner/outer gaps and a 5-μm ring radius to enable measurement of a large 2% strain.

D. Example Strain Determination

Perhaps the best way to convey the procedure and temperature insensitivity of strain determination is via a simulated example using the formulations presented earlier. To this end, TABLE I summarizes the design of the sensor herein with typical values for the starting voltages indicated in Fig. 1. The following analysis assumes there is no fabrication-induced thermal expansion mismatch between the structure and substrate material, i.e., that strain comes only from external sources that induce strain in the substrate to be measured via this device and technique. Here, we start with a substrate tensile strain of 25με at 20°C, which changes the inner and outer electrode-to-resonator gaps by -0.286 nm and +0.437 nm, respectively.

The procedure begins with the plotting of the post-strain resonance frequency versus DC bias curves for two cases: 1) when driving the ring electrode and taking the output from the inner electrode bond pad; and 2) when instead taking the output from the outer electrode bond pad. Fig. 3 presents simulated frequency response curves as a function of DC bias V_P (with V_i=0V and at 20°C) for the two cases, essentially showing the kind of plots that must be measured in an actual strain determination (as done in Section III later). The resonance peaks in these plots then yield the frequency versus DC bias plots for the 20°C case in Fig. 4.

Use of d_{in} and d_{out} as fitting parameters to fit the two curves then yields 79.715 nm and 80.437 nm for the inner and outer gaps (after application of 25με of substrate tensile strain at 20°C). Use of (3) then yields an output strain of 25.00με, exactly as expected.

A more interesting simulation keeps a substrate tensile strain of 25με but changes the temperature to 220°C, effectively simulating the effect of a rather large 200°C temperature shift. The

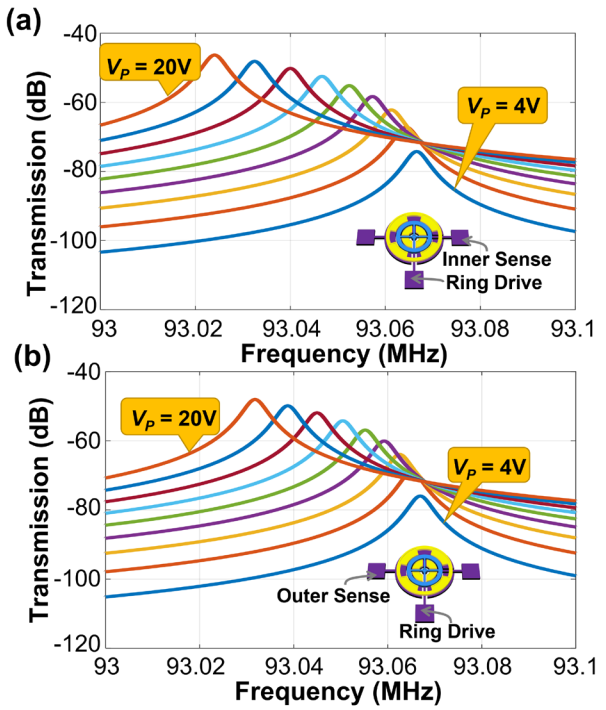

Fig. 3: Simulated frequency spectra for the ring strain sensor as a function of (a) inner and (b) outer port for sensing at a room temperature of 20°C when 25μ tensile strain is introduced to substrate.

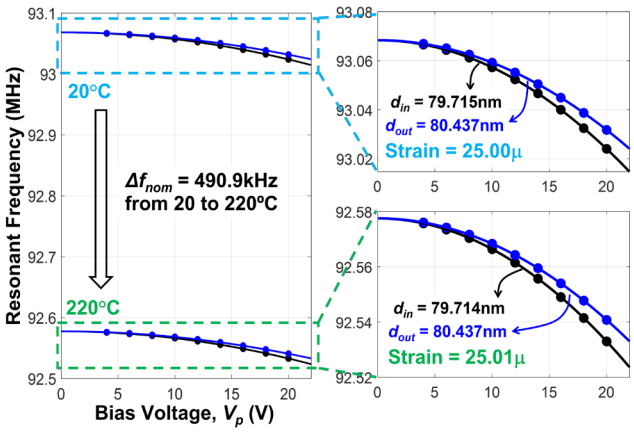

Fig. 4: Wide- and zoomed-view of simulated resonance frequency versus bias voltage curves used to extract inner and outer gap spacings for determination of strain and demonstrate how the measured strain output remains practically the same at 20°C and 220°C, attesting to the temperature insensitivity of this sensor.

curves for this case (also shown in Fig. 4) have shifted more than 490 kHz from the 20°C ones, but their shape remains practically the same. Again, it is the shape of the curve that determines strain, not the intercept point, so the extracted strain of 25.01με changes by an insignificant 0.01με compared to the 20°C case. This corresponds to a remarkably small temperature dependence of only 0.05nε/°C, very clearly attesting to the temperature insensitivity of this strain sensor, at least from a simulation perspective.

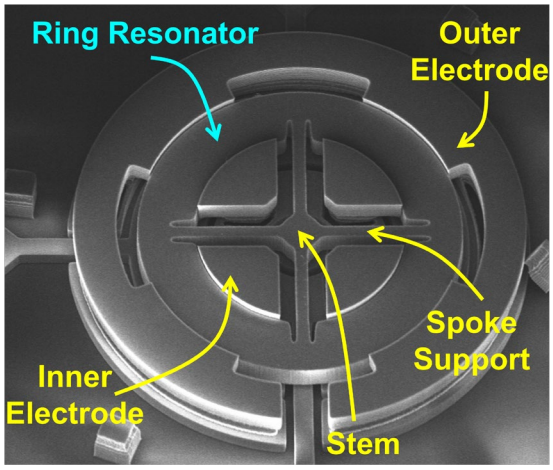

Fig. 5: SEM of a fabricated polysilicon ring resonator strain gauge.

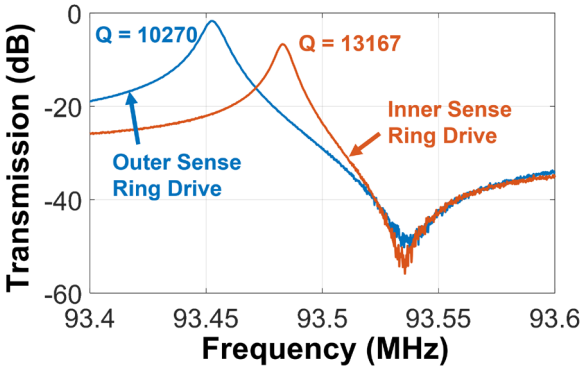

Fig. 6: Measured frequency response spectra of the fabricated polysilicon ring resonator clearly showing the difference when sensing from the inner versus outer electrodes.

III. Measured Results

Fig. 5 presents (a) the SEM image of a fabricated Fig. 1 device using the polysilicon surface micromachining process described in [9]. Fig. 6 presents measured frequency response spectra taken separately from the inner and outer electrodes under 7mTorr vacuum supplied via a Lakeshore temperature controllable vacuum probe station. Curve-fitting (1) to open-loop measured frequency versus (V_P-V_i) (i=1,2) of the ring resonator at 20°C yields initial inner and outer gaps (before application of strain) of d_{in} = 58.68 nm and d_{out} = 50.05 nm, respectively.

Normally, a sensor like affixes to the surface experiencing the strain to be measured, often using an adhesive. This then creates a complex situation where strain on the surface transfers to the adhesive, then to the strain sensor substrate, at which point the measured substrate strain is no longer precisely the same as that of the surface. To avoid uncertainty presented by such a complex interface, this work applies strain directly to the sensor substrate via the apparatus of Fig. 7. This contraption dispenses with any need for adhesives and rather applies strain by bending the substrate die using probes and the topography of the chuck. Here, the die housing the ring resonator sits atop a valley in the chuck with the ring resonator at its center. To

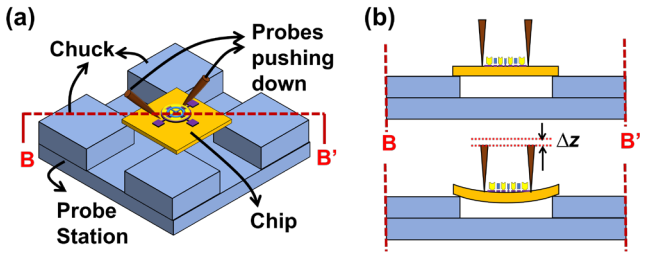

Fig. 7: (a) Strain application via probes. (b) Cross-section along B-B'.

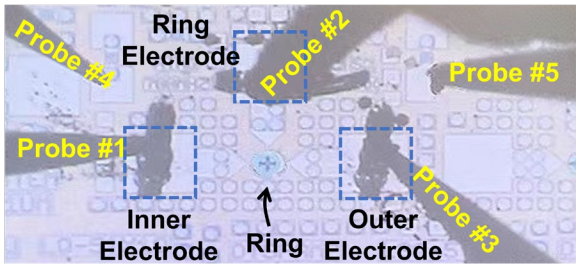

Fig. 8: Optical microscopic photo of probes and ring resonator during strain sensor testing.

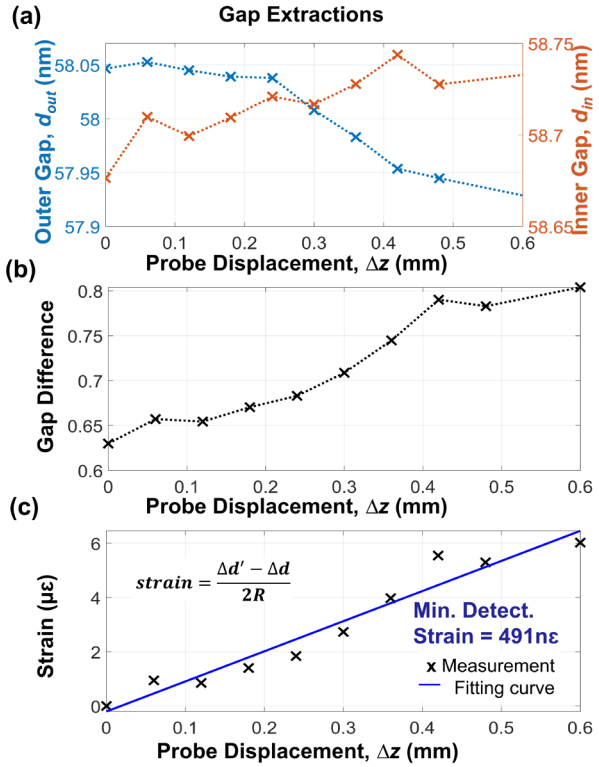

Fig. 9: Measured a) inner and outer gap, b) gap difference, and c) strain output of the ring resonator strain sensor versus probe vertical displacement.

apply strain, two probes push downward on the chip in the proximity of the ring resonator. Fig. 8 shows the microscopic image of the strain gauge under testing. Three probes, #1, #2 and #3, connect to the inner electrode, the ring, and the outer electrode, respectively. Probe pads are metallized to reduce contact resistance and hence minimize load-resistance induced frequency pulling [8]. Two probes, #4 and #5, apply strain to the chip. Here, the strain is proportional to the vertical displacement of

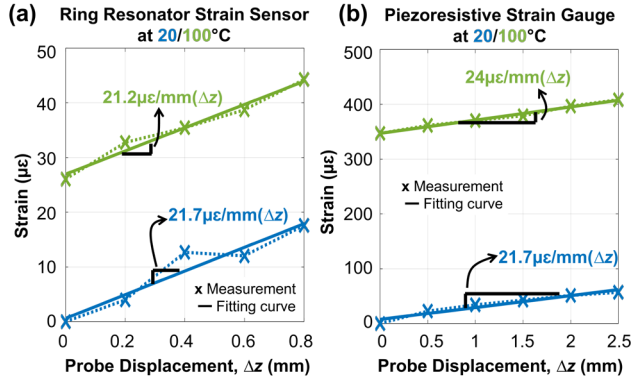

Fig. 10: Measured strain using the (a) ring resonator strain sensor and (b) conventional piezoresistive strain gauge on the same chip versus probe vertical displacement Δz at 20°C and 100°C.

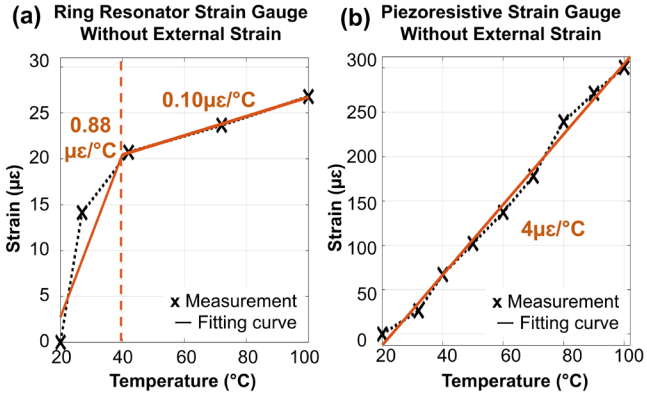

Fig. 11: Measured strain versus temperature of (a) the ring resonator strain sensor and (b) the piezoresistive strain gauge with curve-fits to extract temperature coefficients.

the probe, Δz.

Fig. 9 plots the a) measured inner gap and outer gap, b) measured inner-outer gap difference and c) measured strain output (computed using (3)) versus vertical probe displacement, Δz. So far, the minimum detectable strain is 491 nε using an open-loop frequency measurement method. Though quite good, a closed-loop oscillator approach to frequency determination would likely do even better, with a theoretically predicted resolution down to 9.19 nε [7].

Fig. 10 compares the measured strain versus vertical probe displacement Δz at 20°C and an elevated temperature of 100°C for (a) the electrical stiffness-based ring strain sensor and (b) a conventional polysilicon piezoresistive strain gauge residing on the same chip. Here, the two sensors have similar scale factors, but the ring sensor has far less temperature dependence. Fig. 11(a) and (b) plot measured strain output versus temperature, where the ring sensor experiences a strain excursion of 26.8 με over 20-100°C, which is more than ten times smaller than the 300.5 με of the piezoresistive strain gauge over the same range. The output strain temperature coefficient of 0.1με/°C above 40°C is three times better than [5].

IV. Conclusions

The ability of the described strain sensor to maintain such

low temperature dependence from 40°C to 100°C, and in such a small size, makes it a compelling candidate to enable a vision where strain sensing skins containing ensembles of such sensors might monitor and detect imminent failure of critical mechanical structures, e.g., a hydrogen tank in a fuel cell automobile engine. The work herein evaluated the ring-based sensor open-loop, so did not obtain a good estimate for the ultimate resolution of the sensor, which is best done with closed-loop feedback. The high *Q* over 10,000 of the ring in its fundamental mode does support an expectation that the resolution should be quite good, where theory puts it in the nano-strain range. Efforts pursuant to closing the loop are in progress.

REFERENCES

[1] "Practical Strain Gage Measurements," Omega Engineering,[Online].Available:https://www.omega.co.uk/techref/pdf/StrainGage_Measurement.pdf.

[2] G. R. Higson, "Recent advances in strain gauges," *Journal of Scientific Instruments,* vol. 41, pp. 405-414, 1964; DOI:10.1088/0950-7671/41/7/301.

[3] "SGD-10/350-LY41 Datasheet," Omega Engineering, [Online]. Available: https://assets.omega.com/pdf/test-and-measurement-equipment/strain-gauges/SGD_LINEAR1-AXIS.pdf.

[4] K. Wojciechowski, B. Boser and A. Pisano, "A MEMS resonant strain sensor operated in air," 17th IEEE International Conference on Micro Electro Mechanical Systems. Maastricht MEMS 2004 Technical Digest, Maastricht, Netherlands, 2004.

[5] R. G. Azevedo, D. G. Jones, A. V. Jog, B. Jamshidi, D. R. Myers, L. Chen, X.-a. Fu, M. Mehregany, M. B. J. Wijesundara and A. P. Pisano, "A SiC MEMS Resonant Strain Sensor for Harsh Environment Applications," *IEEE Sensors Journal,* vol. 7, no. 4, pp. 568 - 576, April 2007, DOI: 10.1109/JSEN.2007.891997.

[6] C. D. Do, A. Erbes, J. Yan, K. Soga and A. A. Seshia, "Vacuum Packaged Low-Power Resonant MEMS Strain Sensor," *Journal of Microelectromechanical Systems,* vol. 25, no. 5, pp. 851 - 858, Oct 2016; DOI: 10.1109/JMEMS.2016.2587867.

[7] A. Ozgurluk and C. T. -C. Nguyen, "On-Chip Precision Residual Strain Diagnostic Based on Gap-Dependent Electrical Stiffness," in *2019 20th International Conference on Solid-State Sensors, Actuators and Microsystems & Eurosensors XXXIII (TRANSDUCERS & EUROSENSORS XXXIII)*, Berlin, Germany, June 2019.

[8] M. Akgul, L. Wu, Z. Ren and C. T. Nguyen, "A negative-capacitance equivalent circuit model for parallel-plate capacitive-gap-transduced micromechanical resonators," *IEEE Transactions on Ultrasonics, Ferroelectrics, and Frequency Control,* vol. 61, no. 5, pp. 849-869, May 2014; DOI: 10.1109/TUFFC.2014.2976.

[9] T. L. Naing, T. O. Rocheleau, Z. Ren, S.-s. Li and C. T.-C. Nguyen, "High- Q UHF Spoke-Supported Ring Resonators," *Journal of Microelectromechanical Systems,* vol. 25, no. 1, pp. 11 - 29, Feb 2016; DOI: 10.1109/JMEMS.2015.2480395.

[10] J. Vanhellemont, A. K. Swarnakar and O. V. d. Biest, "Temperature Dependent Young's Modulus of Si and Ge," *ECS Transactions,* vol. 64, no. 11, 2014.